Nuclear Materials and Energy 37 (2023) 101507

Contents lists available at ScienceDirect

Nuclear Materials and Energy

journal homepage: www.elsevier.com/locate/nme

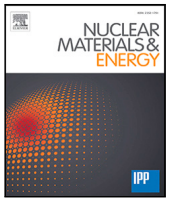

Sputtering yield reduction for nano-columnar W surfaces under D ion irradiation

J. Brötzner [a,*], C. Cupak [a], M. Fellinger [a], H. Biber [a], A. Lopez-Cazalilla [b], F. Granberg [b], F. Kporha [b], A. Mutzke [c], R. González-Arrabal [d], F. Aumayr [a]

[a] Institute of Applied Physics, TU Wien, Wiedner Hauptstraße 8-10/E134, Vienna, 1040, Austria
[b] Department of Physics, University of Helsinki, P.O. Box 43, Helsinki, FI-00014, Finland
[c] Max–Planck Institute for Plasma Physics, Wendelsteinstrasse 1, Greifswald, 17491, Germany
[d] Instituto de Fusión Nuclear "Guillermo Velarde" and Departamento de Ingeniería Energética, ETSI de Industriales, Universidad Politécnica de Madrid, C/ José Gutiérrez Abascal, 2, Madrid, E-28006, Spain

ARTICLE INFO

Keywords:
Tungsten nano-columns
Deuterium
Sputtering
Ray-tracing
BCA

ABSTRACT

This study investigates the sputtering properties of nano-columnar tungsten surfaces under 2 keV D_2^+ irradiation. It was conducted both by performing experiments in a highly sensitive quartz crystal microbalance setup as well as by numerical methods using two simulation codes called SPRAY and SDTrimSP-3D. A key question was whether the strong sputtering yield reduction observed in previous studies under 2 keV Ar^+ irradiation is maintained when using a much lighter ion species like deuterium. For the latter, a substantially larger projected range in the material has to be expected. Therefore, a total confinement of the ion-solid interaction within the W nano-columns cannot be assumed *a priori*. However, both the experiments and the numerical simulations showed in good agreement that the geometrically induced sputtering yield reduction is still observed to the same extent despite the increased range of ions in the material. Thus, a potential application of such nano-columnar tungsten surfaces as plasma facing components in future nuclear fusion devices is not affected.

1. Introduction

For thermonuclear fusion devices, the availability of suitable first wall materials that can withstand the harsh physical conditions present inside a reactor vessel is a critical requirement for achieving mankind's goal of developing a viable fusion power plant concept [1]. Especially the divertor is a critical plasma-facing component (PFC) where very high particle fluxes and heat loads are present during operation. On the divertor foreseen in ITER, which is the largest thermonuclear fusion experimental reactor currently under construction in the south of France, stationary thermal heat loads of ~10 MW/m^2, short transient heat loads up to GW/m^2 during edge-localised modes (ELMs) and large fluxes of energetic particles reaching up to $\sim 5 \times 10^{23}$ m^{-2}s^{-1} are expected [2,3]. A prominent material choice for the divertor is tungsten (W), which is the metal with the highest known melting temperature. A further advantage of W is a relatively low sputtering yield when irradiated with energetic plasma particles, which increases the expected lifetime of the divertor while decreasing the impurity concentration in the main plasma region. The latter is important to keep radiative losses from the plasma low, allowing a higher energy gain. These properties support the suitability of W as the first wall material for a divertor. The use of W as a divertor material has already been successfully demonstrated in state-of-the-art experiments like ASDEX-Upgrade [4] or JET [5] and is also foreseen in ITER [2]. Nevertheless, the scientific community working on plasma–wall interaction (PWI) is continuously investigating new materials and their behaviour under exposure to energetic particles in order to provide the necessary technological basis and knowledge to realise the first commercial nuclear fusion power plant.

In recent studies, the potential use of nano-engineered W surfaces for PFCs instead of conventional flat W gained some attention, as several favourable properties could be observed. For instance, a reduction of W-fuzz growth rates during exposure of nano-columnar W (NCW) surfaces to He plasmas was identified in a study by Qin et al. [6]. Also, beneficial properties like reduced thermal stresses when exposed to localised heat loads were observed [7]. Furthermore, a substantial sputtering yield reduction was recently identified via both experiments and numerical simulations for the case of NCW irradiation under Ar^+ bombardment [8]. Similar results were already observed in an earlier work by Ziegler et al. for nano-structured W surfaces under

* Corresponding author.
E-mail address: broetzner@iap.tuwien.ac.at (J. Brötzner).

https://doi.org/10.1016/j.nme.2023.101507
Received 3 July 2023; Received in revised form 4 September 2023; Accepted 8 September 2023
Available online 14 September 2023

He ion irradiation [9]. Recently, a numerical optimisation study by Cupak et al. indicated a specific geometrical NCW configuration which allows for a favourable reduction of the 2 keV Ar^+-induced sputtering yield for irradiation along the surface normal direction down to 20% with respect to flat W [10]. Such results in principle motivate further investigations of these complex topographies for potential applications of NCW as PFC.

The sputtering yield reductions as reported in previous work focusing on Ar^+ irradiation were directly attributed to geometric effects caused by the NCW topography. This special surface structuring enhances redeposition of sputtered W and also reduces the sputtering yield dependence on parameters like the ion incidence angle [8]. However, one critical question for a potential application in a nuclear fusion reactor is whether these findings are also applicable if lighter projectiles like deuterium (D), which as a fuel species is more fusion-relevant, are selected for the irradiation of NCW. In contrast to Ar, D has a much lower stopping power and therefore a larger mean projected ion range r_p in W. The previously observed sputtering yield reduction could be explained by a simple geometric model in which the sputtering characteristics of a flat surface were mapped onto the surface of a sample of interest while neglecting the actual cascades of individual collisions occurring within the solid. This assumption might however be daring in the deuterium case where the projectiles reach farther into the sample columns, which themselves are limited in their geometric dimensions. It is thus of interest to test the sputtering properties of NCW surfaces also during irradiation with light projectiles.

To this end, we present the following study which includes sputtering yield measurements of real NCW surfaces under 2 keV D_2^+ bombardment using a highly sensitive quartz crystal microbalance (QCM) setup, but also numerical simulations employing the geometric ray-tracing code SPRAY [11] and the full 3D BCA code SDTrimSP-3D [12]. With data from these different techniques at hand, we can go beyond a mere geometric model and untangle the further contributions to a possible reduction in sputtering yield, if present. The key goal is therefore to elucidate if and to what extent this favourable sputtering reduction effects as observed under Ar^+ irradiation holds when considering much lighter fuel species.

2. Materials and methods

2.1. Experimental methods and choice of samples

Experimental sputtering yield data were obtained using a high-precision quartz crystal microbalance (QCM) setup. In this technique, an SC-cut quartz resonator is driven in a thickness shearmode oscillation and its resonance frequency is tracked using specialised electronics [13]. Based on the foundation laid by Sauerbrey in [14], small mass changes Δm of the resonator are related to changes of its resonance frequency Δf via Eq. (1).

$$\frac{\Delta m}{m_0} = -\frac{\Delta f}{f_0} \tag{1}$$

Here, m_0 and f_0 denote the original mass and eigenfrequency of the QCM, respectively. Eq. (1) remains valid also for thin films of foreign material deposited onto the QCM, allowing to study in real time the erosion of samples that have been grown directly onto the quartz platelet. In past studies, this very setup has been shown to be capable of resolving mass change rates of up to 10^{-4} monolayers of W per second [15].

For this investigation, tungsten NCs were grown directly onto quartz resonators by means of DC magnetron sputtering under oblique angle (zenithal deposition angle of 85°). An Al mask was used during the deposition process to ensure that not the whole QCM area was covered, thereby preventing possible electrical shorts of the planar QCM electrodes. The topography of the NCW layer was characterised, prior to and after the sputtering experiments, using high resolution field emission gun — scanning electron microscopy (SEM). The mean diameter of the columns and their height were determined to be 50 ± 10 nm and 665 ± 8 nm, respectively, while they cover approximately 58% of the deposited surface. Figs. 1a and 1b show top view and cross sectional SEM images of the NCW, respectively. The oblique appearance of the columns in Fig. 1a is caused by the SEM detector being positioned off-centre from the surface normal direction, while Fig. 1b shows the parallel nature of the W nano-columns with respect to the global sample surface normal. Samples were taken from the same batch studied previously in [8], where their production and the analyses are described in greater detail. Additionally to these microscopy images, a computer model of the nano-structures was generated, taking into account the geometric dimensions from the above described analyses. The diameter was fixed at 50 nm while the height of the individual columns was varied by $\delta h \leq \pm 50$ nm around a mean of 500 nm to better represent the measured columnar height distribution. According to [10], no further reduction in sputtering yield is to be expected with increasing column height and fixed surface coverage density and column diameter. Moreover, simulations with different mean height values down to 400 nm did not show significantly different results, thus justifying the discrepancy in column height between SEM studies and models. The cylinder tops were terminated with cones, mimicking the tips seen in Fig. 1b. A render of the model is given in Fig. 1c.

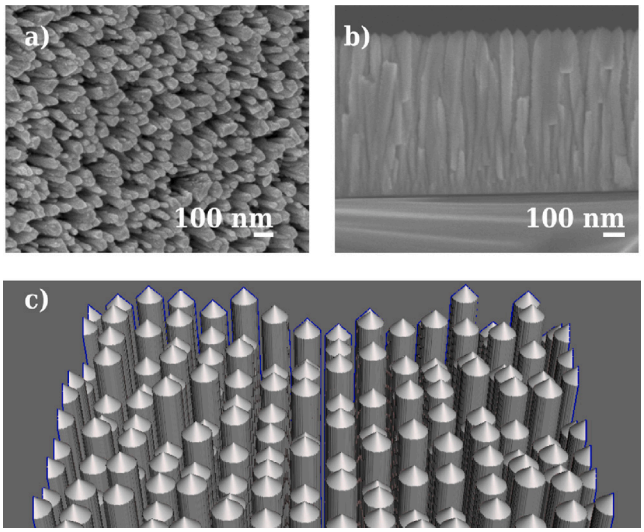

Fig. 1. Top view (a) and cross-sectional view (b) as imaged by SEM of nano-columnar tungsten grown on a Si substrate with an Au inter-layer. c) Representation of a computer generated model of the nano-columns to be used as input for simulations. Images adapted from [8].

Irradiations of the coated QCM were carried out under ultra-high vacuum conditions with a base pressure of 1×10^{-9} mbar. The sample was placed on a rotatable manipulator allowing to tilt it with respect to the ion beam. Data were obtained for incidence angles ranging from 0° to 70° in 5° increments, where by convention angles are measured with respect to the target surface normal. Ions were extracted from an all-permanent magnet electron cyclotron resonance ion source [16] in the form of 2 keV D_2^+ as a proxy for 1 keV D^+. Using molecular deuterium, higher fluxes of 7.72×10^{16} ions/m^2/s were achieved compared to atomic deuterium. The ion beam current density was checked by means of a Faraday cup both before and after the irradiations to ensure constant experimentation conditions. Literature shows that at these velocities, no effects due to the molecular structure of the projectile are to be expected [17,18]. This can be understood as follows: The 2 keV molecular deuterium ion dissociates at the surface. Both individual atomic D retain energies of about 1 keV because the dissociation energy of D_2 is of the order of 10 eV at most and therefore negligible compared

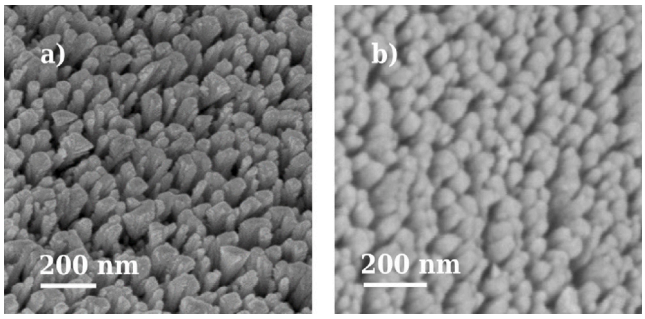

Fig. 2. SEM image taken before (a) and after (b) irradiation. The nano-columns are still present and no erosion is discernible.

to the involved kinetic energies [19]. Inside the solid, their trajectories are governed by random walk processes and the two collision cascades evolve independently and become spatially separated after a few collisions. Experimentally obtained sputtering yields for 2 keV D_2^+ were therefore divided by 2 to represent data for 1 keV D^+.

To verify that the sputtering and reflection of D_2 is indeed the same as twice the values of D with the same energy per nucleon, molecular dynamics (MD) simulations were carried out with PARCAS [20,21]. Because MD can consider the molecular projectile structure, it is a suitable means to validate this link between experiments with molecular ion beams and simulation codes that deal with atomic projectiles (see Section 2.2). We investigated perpendicular irradiation and irradiation at 60° incidence. The total distance the ion could travel in the MD cell was comparable with the observed penetration depth. 40,000 projectiles were simulated at perpendicular impact and 20,000 impacts at 60°, to obtain statistics. We used the interatomic potentials by [22]. Reflection yields were found to be practically identical, considering the factor of two between D and D_2 at both incidence angles. The sputtering yields were also similar when accounting for the factor two. However, the very low sputtering yield resulted in some variation, with the final values for D being ~40% of the ones for D_2 rather than the expected 50%. We do still keep the scaling factor of 0.5, since it lies within the numerical uncertainty and because of the available literature [17,18]. Moreover, it gives a more conservative estimation for erosion and lifetime considerations.

Under this assumption, the flux of 7.72×10^{16} $D_2^+/m^2/s$ corresponds to 1.54×10^{17} $D^+/m^2/s$. Given the tabulated surface coverage density of 6.3×10^{15} $W/cm^2/nm$ for tungsten and a nano-column surface coverage of ~50%, 1 nm depth of NCW can then be roughly approximated to contain 3.15×10^{19} W/m^2 atoms. Integrating the deuterium flux over all irradiation times results in a total applied fluence of 7.5×10^{21} D^+/m^2. With a sputtering yield of approximately 5×10^{-3} W/D (see Section 3), this corresponds to the erosion of roughly 1 nm over the whole course of the experiments. Therefore, a steady-state sputtering yield can be measured without having to account for fluence dependent erosion processes. This is furthermore corroborated by SEM images, which show no difference in the NCW morphology before and after sputtering, as is given in Fig. 2.

2.2. Simulation approach

To model the sputtering of solids, a common tool are computer simulations based on the binary collision approximation (BCA) [23]. In these codes, usually an amorphous solid is assumed and the trajectories of the projectiles are tracked through the sample. After a mean free path determined by the sample density, an elastic collision between the projectile and a single recoil is assumed to happen, for which momentum and energy transfer are calculated according to classical scattering theory. Inelastic energy loss is accounted for during the particles' paths between collisions. After the recoil (and all subsequent recoils) are set in motion, their trajectories and energies are also tracked, until their energies fall below a certain threshold and the particles are considered stopped. Thus, the ensuing collision cascade is monitored. This allows to obtain insight on the sputtering yield and the angular distribution of ejecta, as well as mean projected ranges of the projectiles inside the target, among others. Moreover, BCA codes are considerably faster than MD, for which some technical issues need to be considered. Therefore, BCA is the method of choice for this study [24].

In this study, we used the following BCA based codes: SDTrimSP [25] and SDTrimSP-3D [12]. SDTrimSP is a one-dimensional simulation software, meaning targets are assumed to have an infinite flat surface while material properties like concentrations or ion beam induced damages are functions of depth only. Particularly, sputtering yield data for flat reference samples were obtained from SDTrimSP with a convenient and user-friendly graphical user interface [26], using static simulations and the default input parameters ("H, D, T" inelastic loss model, tabulated surface binding energy of W, KrC interaction potential and Gauss–Legendre integration). In contrast, SDTrimSP-3D can operate on almost arbitrary sample geometries for which the surface can be specified in all three spatial dimensions. Modelling of the NCW was performed with SDTrimSP-3D using the computer generated images for the W columns that were described in Section 2.1. These model surfaces have already been shown to better reproduce experimental data with argon projectiles compared to microscopy images [8]. The advantage of using SDTrimSP-3D for this particular geometrical configuration is that it allows calculating the collision cascade fully in three dimensions. Since no significant erosion was observed during D bombardment, SDTrimSP-3D was run in the static mode to reduce calculation time. Nonetheless, these simulations still come with the downside of computationally high demands (≳100 GB of random-access memory) and long runtimes (several days).

Therefore, sputtering yields were also simulated with the SPRAY code [11]. It takes as input both the surface topography of the sample to be investigated and a database of sputtering data for flat surfaces, generated usually from one-dimensional BCA simulations. Surface geometries can be loaded from either microscopy images, or from computer generated models. In this case, the models shown in Fig. 1c were used, just like for the SDTrimSP-3D simulations. The repository data on the sputtering of flat surfaces contains information on the sputtering yield and the trajectories of sputtered atoms and reflected ions, both as a function of incidence angle and impactor energy. By means of ray-tracing, the projectile trajectories are tracked onto the target where the local conditions of the impact are checked. For these locally prevalent conditions, particles and ions are assumed to be sputtered and reflected, respectively, according to the aforementioned repository data. Further tracing of the newly generated particles allows to simulate the effects of ion reflection, secondary sputtering and redeposition of ejecta as well as automatically considering a variation of the local incidence angle as well as shadowing of affected surface regions. These simplifications of the simulated model significantly reduce computational demands.

3. Results and discussion

Fig. 3 shows the sputtering yields as a function of incidence angle obtained from simulations and experiments for bombardment of W in both the flat and nano-columnar configurations with 1 keV D^+ ions. The simulated sputtering yield for flat tungsten is given by the blue solid line and observed to start at roughly 0.008 W/D under normal incidence, after which it increases with the incidence angle θ with respect to the target surface normal until a maximum of 0.021 W/D is reached at $\theta \approx 80°$. At larger angles, the sputtering yield decreases again and drops to 0 at $\theta \approx 85°$ due to increased projectile reflection at grazing incidence. A different trend is observed, however, for the W nano-columns. SPRAY simulations (green curve) report sputtering yields starting at 0.005 W/D at $\theta = 0°$ and reaching 0.01 W/D at $\theta = 80°$ incidence, respectively. The sputtering yield is drastically reduced by

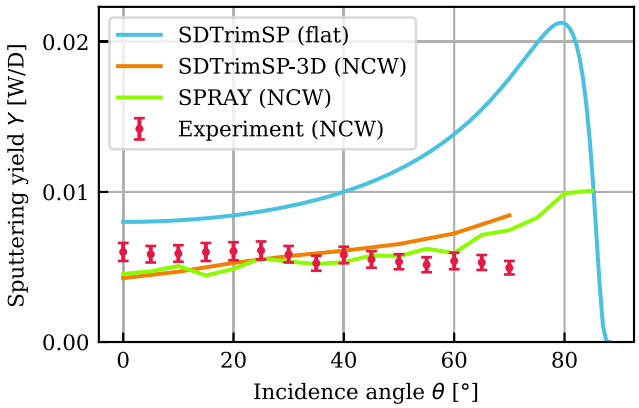

Fig. 3. Sputtering yields of W under 1 keV D^+ impingement as a function of incidence angle with respect to the target surface normal. Simulations were carried out using SDTrimSP for a flat sample (blue) and SDTrimSP-3D and SPRAY for tungsten nano-columns (orange and green, respectively). Experimental data are shown by red dots. 0° denotes normal incidence.

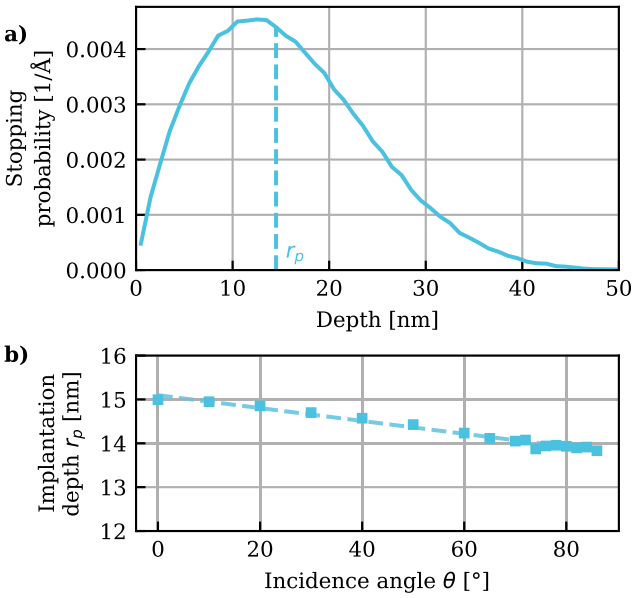

Fig. 4. (a) Range of 1 keV D in W given as the stopping probability of a projectile ion as function of depth. Shown for irradiation along the surface normal direction. The dashed vertical line denotes the mean projected ion range r_p. (b) Mean projected ion range for various incidence angles. The decrease towards more grazing incidences follows a linear trend, as is indicated by the fit function represented by the dashed line. Data were obtained using the SDTrimSP code [25,26].

a factor of about 2 in the whole studied θ range and depends only weakly on the angle of incidence. SDTrimSP-3D data presented in orange confirm the quantitative values obtained from SPRAY as well as the trend of a flattened and less pronounced behaviour over the incidence angle. Also the experimental results given by the red dots show a sputtering yield reduction with respect to the flat surface. For θ in the range between 20°–60°, both simulated data and experimental results for the NCW coincide with the error bars. For more normal and more grazing incidences, the measured yields are underestimated and overestimated by the simulations, respectively. Almost no angular dependence of the sputtering yield is resolved experimentally.

These results qualitatively agree with those reported for 1 keV and 2 keV Ar^+ bombardment, where the flattening of the angular dependence was attributed to the surface envelope roughness and the lowering to redeposition within the hollow channels [8]. Quantitatively, however, the measured sputtering yield of 1 keV D^+ of 0.005 W/D is smaller than for 1 keV Ar^+ by a factor of roughly 100. We further quantified this difference in sputtering yield of D^+ and Ar^+ of 1 keV energy each: For all experimentally covered incidence angles (0°–70°, 5° increments), we took the ratio between sputtering yields of both D and Ar point-wise at each angle and calculated their mean and standard deviation. This reduction factor is $(9.3\pm1.5)\times10^{-3}$ for the experimentally measured sputtering yields, while it is $(8.4\pm1.0)\times10^{-3}$ and $(8.1\pm2.7)\times10^{-3}$ for SPRAY and flat SDTrimSP simulations, respectively. Thus, the reduction when choosing deuterium as projectile remains the same, regardless of whether nano-columnar or flat surfaces are considered. For flat samples, this effect can be ascribed to the lower mass and therefore lower momentum transfer from the D ions to the W target atoms. Moreover, due to the higher implantation depth, collisions take place deeper in the sample. This leads to a decreased likelihood of particles being released from the near-surface regions. While the mass effect stays the same for both surface types, the increased implantation range could potentially lead to different effects due to the confined nature of the columns. However, the observation that the reduction in sputtering yield does not change for the nano-column structure suggests that the nano-structuring affects the results from both projectile species equally.

This can be understood by a more in-depth consideration of the respective ion penetration depths. The stopping probability of 1 keV D projectiles as simulated by SDTrimSP is given by the solid line in Fig. 4a, while the dashed blue line gives the mean projected range r_p. Despite being roughly an order of magnitude bigger than what is calculated for the 2 keV Ar^+ used in [8], it is still within the mean diameter of the tungsten nano-columns. Moreover, the distribution decays rapidly enough such that its tail towards higher implantation depths decays sufficiently fast so that no implantation is probable beyond the mean NCW diameter of 50 nm. Therefore, transmission through the columns in the direction normal to the column centre axis can be considered negligible. For other directions, the behaviour of the mean projected ion range r_p is given in Fig. 4b. For more grazing incidence angles, it decreases linearly as indicated by the dashed line that is a fit function through square data points. Furthermore, with increasing incidence angle, also the probability of projectile reflection increases. Therefore, under oblique incidence the probability for ion transmission, an effect not covered by our purely geometric SPRAY simulations, decreases and for the whole range of possible incoming ion directions, ion transmission is expected to be a minor effect.

Another strong indicator for the applicability of a geometric treatment during the studied sputtering processes is the remarkable agreement between the two different three-dimensional simulations, SDTrimSP-3D and SRPAY, which are given by the orange and green curves in Fig. 3. While SPRAY trades in the complexity of its underlying assumptions for computational efficiency and a reduction of runtime, SDTrimSP-3D does not. The shortcomings in modelling used by SPRAY are a lack of dynamic calculations and a purely geometrical treatment of the irradiated surface, neglecting the formation of a collision cascade inside the target. Nonetheless, both codes' results match, which thus allows for the following conclusions: Firstly, the irradiation of the NCW with 1 keV D^+ ions under the reported conditions, especially the low ion fluxes, can be treated statically. This is due to the inherently low sputtering yield of tungsten, especially when bombarded with light ion species. Moreover, once a steady state sputtering yield is reached in the experiment, no variation of the sputtering yield as a function of applied fluence is observed. This assumption has also been verified by means of SEM measurements post irradiation as shown in Fig. 2. Secondly, as the omission of a numerical treatment of processes inside the target does not lead to a different result, the sputtering of this specific projectile–target combination can still be described using the surface geometry alone, as is done in SPRAY. Justification for this was given above in the treatment of the ion implantation ranges governing the length scales of

ion-driven modifications inside the solid compared to the dimensions of the NCW.

We therefore conclude that the reduction in sputtering yield through nano-structuring that is predicted by computer simulations and confirmed by experiments can be explained solely by a basic geometric consideration of the target surface morphology.

The long-term stability of this desirable yield reduction remains an open question, however. Using similar estimations as sketched in Section 2.1, a fluence in the order of 10^{24} D/m^2 would be necessary for full erosion under the assumption of a sputtering yield of 0.005 W/D and 500 nm high nano-pillars. This estimate is based on the static conditions that were justified for this study, but might have to be modified for substantial erosion. When the impactor energy is lowered towards the sputtering threshold of W (~250 eV), SDTrimSP predicts a sputtering yield reduction for D impact of roughly three orders of magnitude. Whether this is enough for the NCW structure to survive the expected plasma conditions in fusion devices like ITER remains to be investigated. First dynamic investigations have been carried out for 2 keV Ar^+ as projectiles [10]. In this case, numerical treatment in a reasonable time span is possible due to the much higher sputtering yield. For the significantly lighter deuterium, however, these investigations still pose a computational challenge for future research.

4. Summary and conclusion

In this study we investigated the sputtering yield of nano-columnar tungsten under 1 keV D^+ ion impact combining both experiments and simulations. Such nano-structured W surfaces have been shown in the past to reduce the sputtering yield of both 1 keV and 2 keV Ar^+ projectiles, thus possibly enhancing lifetimes of PFCs [8]. To investigate whether this effect persists under deuterium bombardment, we measured the sputtering yields as a function of incidence angle using a quartz crystal microbalance setup. 2 keV D_2^+ served as proxy for 1 keV D^+. Additionally, the irradiation was modelled using the codes SDTrimSP-3D and SPRAY, differing in their underlying models. All methods report the desired decrease in sputtering yield. Simulations further predict a less pronounced behaviour as a function of incidence angle and experiments in fact demonstrate the sputtering yield to be almost independent from the incidence angle.

We conclude that previous findings, according to which description of sputtering processes can be reduced to geometrical models, still hold for the case of 1 keV D^+ as projectile. Despite greater penetration depths than similarly energetic Ar ions, the deuterium's interaction with the target is still confined entirely within the columnar structures. This justifies a treatment based on results from flat surfaces mapped onto the topography of the tungsten columns. The structuring of tungsten in highly corrugated and also oriented ways might therefore be advantageous to prolong the lifetime of plasma-facing components, as it reduces material erosion not only under seeding gas, but also under fuel species irradiation.

CRediT authorship contribution statement

J. Brötzner: Methodology, Investigation, Data curation, Visualization, Formal analysis, Writing – original draft. **C. Cupak:** Conceptualization, Methodology, Investigation, Software, Writing – original draft. **M. Fellinger:** Investigation, Validation, Writing – review & editing. **H. Biber:** Software, Writing – review & editing. **A. Lopez-Cazalilla:** Conceptualization. **F. Granberg:** Software, Investigation, Writing – review & editing. **F. Kporha:** Software, Investigation, Writing – review & editing. **A. Mutzke:** Software, Resources. **R. González-Arrabal:** Conceptualization, Investigation, Resources, Writing – review & editing. **F. Aumayr:** Conceptualization, Supervision, Resources, Funding acquisition, Writing – review & editing.

Declaration of competing interest

The authors declare that they have no known competing financial interests or personal relationships that could have appeared to influence the work reported in this paper.

Data availability

Data will be made available on request.

Acknowledgements

This work has been carried out within the framework of the EUROfusion Consortium, funded by the European Union via the Euratom Research and Training Programme (Grant Agreement No 101052200—EUROfusion). Views and opinions expressed are however those of the author(s) only and do not necessarily reflect those of the European Union or the European Commission. Neither the European Union nor the European Commission can be held responsible for them. Financial support has also been provided by KKKÖ (commission for the coordination of fusion research in Austria at the Austrian Academy of Sciences – ÖAW). Computer time granted by the IT Center for Science—CSC—Finland and the Finnish Grid and Cloud Infrastructure (persistent identifier urn:nbn:fi:research-infras-2016072533) is gratefully acknowledged. The research leading to these results has partially received funding from the Spanish Ministry of Science and Innovation, through the project RADIAFUS V, Grant No. PID2019-105325RB-C32, and the Comunidad de Madrid (CAM) Convenio Plurianual con la Universidad Politécnica de Madrid en la línea de actuación Programa de Excelencia para el Profesorado Universitario of the CAM. The authors also acknowledge TU Wien Bibliothek for financial support through its Open Access Funding Programme.

References

[1] J. Knaster, A. Moeslang, T. Muroga, Materials research for fusion, Nat. Phys. 12 (2016) 424–434.
[2] R. Pitts, X. Bonnin, F. Escourbiac, H. Frerichs, J.P. Gunn, T. Hirai, A.S. Kukushkin, E. Kaveeva, M.A. Miller, D. Moulton, V. Rozhansky, I. Senichenkov, E. Sytova, O. Schmitz, P.C. Stangeby, G.D. Temmerman, I. Veselova, S. Wiesen, Physics basis for the first ITER tungsten divertor, Nucl. Mater. Energy 20 (2019) 100696.
[3] M. Wirtz, J. Linke, T. Loewenhoff, G. Pintsuk, I. Uytdenhouwen, Transient heat load challenges for plasma-facing materials during long-term operation, Nucl. Mater. Energy 12 (2017) 148–155.
[4] R. Neu, G. Arnoux, M. Beurskens, V. Bobkov, S. Brezinsek, J. Bucalossi, G. Calabro, C. Challis, J.W. Coenen, E. de la Luna, P.C. de Vries, R. Dux, L. Frassinetti, C. Giroud, M. Groth, J. Hobirk, E. Joffrin, P. Lang, M. Lehnen, E. Lerche, T. Loarer, P. Lomas, G. Maddison, C. Maggi, G. Matthews, S. Marsen, M.-L. Mayoral, A. Meigs, P. Mertens, I. Nunes, V. Philipps, T. Pütterich, F. Rimini, M. Sertoli, B. Sieglin, A.C.C. Sips, D. van Eester, G. van Rooij, JET-EFDA Contributors, First operation with the JET international thermonuclear experimental reactor-like wall, Phys. Plasmas 20 (2013) 056111.
[5] S. Brezinsek, A. Kirschner, M. Mayer, A. Baron-Wiechec, I. Borodkina, D. Borodin, I. Coffey, J. Coenen, N. den Harder, A. Eksaeva, et al., Erosion, screening, and migration of tungsten in the JET divertor, Nucl. Fusion 59 (2019) 096035.
[6] W. Qin, F. Ren, R. Doerner, G. Wei, Y. Lv, S. Chang, M. Tang, H. Deng, C. Jiang, Y. Wang, Nanochannel structures in W enhance radiation tolerance, Acta Mater. 153 (2018) 147–155.
[7] A. Terra, G. Sergienko, M. Gago, A. Kreter, Y. Martynova, M. Rasiński, M. Wirtz, T. Loewenhoff, Y. Mao, D. Schwalenberg, L. Raumann, J.W. Coenen, S. Moeller, T. Koppitz, D. Dorow-Gerspach, S. Brezinsek, B. Unterberg, C. Linsmeier, Microstructuring of tungsten for mitigation of ELM-like fatigue, Phys. Scr. 2020 (2020) 014045.
[8] A. Lopez-Cazalilla, C. Cupak, M. Fellinger, F. Granberg, P.S. Szabo, A. Mutzke, K. Nordlund, F. Aumayr, R. González-Arrabal, Comparative study regarding the sputtering yield of nanocolumnar tungsten surfaces under Ar^+ irradiation, Phys. Rev. Mater. 6 (2022) 075402.
[9] J. Ziegler, J.J. Cuomo, J. Roth, Reduction of ion sputtering yield by special surface microtopography, Appl. Phys. Lett. 30 (1977) 268–271.
[10] C. Cupak, A. Lopez-Cazalilla, H. Biber, J. Brötzner, M. Fellinger, F. Brandstätter, P.S. Szabo, A. Mutzke, F. Granberg, K. Nordlund, R. González-Arrabal, F. Aumayr, Sputter yield reduction and fluence stability of numerically optimized nanocolumnar tungsten surfaces, Phys. Rev. Mater. 7 (2023) 065406.

[11] C. Cupak, P.S. Szabo, H. Biber, R. Stadlmayr, C. Grave, M. Fellinger, J. Brötzner, R.A. Wilhelm, W. Möller, A. Mutzke, M. Moro, F. Aumayr, Sputter yields of rough surfaces: Importance of the mean surface inclination angle from nano- to microscopic rough regimes, Appl. Surf. Sci. 570 (2021) 151204.
[12] U. van Toussaint, A. Mutzke, A. Manhard, Sputtering of rough surfaces: a 3D simulation study, Phys. Scr. 2017 (2017) 014056.
[13] G. Hayderer, M. Schmid, P. Varga, H. Winter, F. Aumayr, A highly sensitive quartz-crystal microbalance for sputtering investigations in slow ion–surface collisions, Rev. Sci. Instrum. 70 (9) (1999) 3696–3700.
[14] G. Sauerbrey, Verwendung von Schwingquarzen zur Wägung dünner Schichten und zur Mikrowägung, Z. Phys. 155 (1959) 206–222.
[15] A. Golczewski, K. Dobes, G. Wachter, M. Schmid, F. Aumayr, A quartz-crystal-microbalance technique to investigate ion-induced erosion of fusion relevant surfaces, Nucl. Instrum. Methods Phys. Res. B 267 (4) (2009) 695–699.
[16] E. Galutschek, R. Trassl, E. Salzborn, F. Aumayr, H. Winter, Compact 14.5 GHz all-permanent magnet ECRIS for experiments with slow multicharged ions, in: J. Phys. Conf. Ser., Vol. 58, IOP Publishing, 2007, p. 395.
[17] K. Dobes, P. Naderer, N. Lachaud, C. Eisenmenger-Sittner, F. Aumayr, Sputtering of tungsten by N+ and N2+ ions: investigations of molecular effects, Phys. Scr. 2011 (T145) (2011) 014017.
[18] C. KenKnight, G. Wehner, Sputtering of metals by hydrogen ions, J. Appl. Phys. 35 (2) (1964) 322–326.
[19] G. Herzberg, A. Monfils, The dissociation energies of the H2, HD, and D2 molecules, J. Mol. Spectrosc. 5 (1–6) (1961) 482–498.
[20] K. Nordlund, M. Ghaly, R. Averback, M. Caturla, T.D. de La Rubia, J. Tarus, Defect production in collision cascades in elemental semiconductors and fcc metals, Phys. Rev. B 57 (13) (1998) 7556.
[21] M. Ghaly, K. Nordlund, R. Averback, Molecular dynamics investigations of surface damage produced by kiloelectronvolt self-bombardment of solids, Phil. Mag. A 79 (4) (1999) 795–820.
[22] N. Juslin, P. Erhart, P. Träskelin, J. Nord, K.O. Henriksson, K. Nordlund, E. Salonen, K. Albe, Analytical interatomic potential for modeling nonequilibrium processes in the W–C–H system, J. Appl. Phys. 98 (12) (2005) 123520.
[23] R. Behrisch, W. Eckstein, Sputtering By Particle Bombardment: Experiments and Computer Calculations from Threshold to MeV Energies, Vol. 110, Springer Science & Business Media, 2007.
[24] W. Eckstein, H.M. Urbassek, Computer simulation of the sputtering process, in: Sputtering By Particle Bombardment: Experiments and Computer Calculations from Threshold To MeV Energies, in: Topics in Applied Physics, Springer, Berlin, Heidelberg, 2007, pp. 21–31.
[25] A. Mutzke, R. Schneider, W. Eckstein, R. Dohmen, K. Schmid, U. von Toussaint, G. Badelow, SDTrimSP Version 6.00, IPP-Report Max-Planck-Institut für Plasmaphysik, 2019.
[26] P. Szabo, D. Weichselbaum, H. Biber, C. Cupak, A. Mutzke, R. Wilhelm, F. Aumayr, Graphical user interface for SDTrimSP to simulate sputtering, ion implantation and the dynamic effects of ion irradiation, Nucl. Instrum. Methods Phys. Res. B. 522 (2022) 47–53.